EMS: Biomedical Sciences
University of Edinburgh
Honours Project

Neuroscience
2022-23

Oestrous Cycle-Dependent Modulation of Cortical & Hippocampal Neuronal Activity

Laboratory / Clinical Project

Contents

[Word Count] Abstract [**172**] Lay Abstract [**186**] Contents [**4568**]

Acknowledgements

Surgical procedures and post-hoc confirmation of *Neuropixels* probe location were performed by Arthur Zhang and assisted by Dr Tom Flossmann at the Rochefort Lab. Patricia Maeso Hernandez and I obtained and produced vaginal photographs and vaginal smear histologies. Data analysis was performed by Dr Zahid Padamsey, a principal investigator at Cambridge, Arthur Zhang, and myself. A python-based analysis pipeline (sourced from the Duguid lab) was used to analyse electrophysiological data.

I would like to sincerely thank Patri Maeso Hernandez, Dr Alfredo Llorca, Dr Tom Flossmann, Arthur Zhang, Dr Danai Katsanevaki, Dr Nina Kudryashova, and Zihao Chen, and in particular, Professor Nathalie Rochefort, of the Rochefort Lab for welcoming me to with warmth and providing me with endless support and guidance. I have learned so many valuable lessons from each and every one of you and am extremely grateful for the time spent with everyone throughout this project.

To Yoshimi, Kyun, Diya, Kaisa, Sara, Anoukia, Daniel, mentors in music, and my parents—thank you for supporting me with everything that I do.

Abstract

Changes in behaviour and cognitive function have been reported to correlate with sex hormone fluctuations in female mammals. Prior studies have used visual behaviours to clarify how reproductive cycles influence brain and behaviour. However, it is still unclear how sex hormone fluctuations mechanistically regulate information processing in the mammalian brain.

In this project, young female mice were presented with visual stimuli and the activity of their primary visual cortex (V1) and hippocampal formation (HPF), recorded with chronic high-density and large-scale *in vivo* extracellular silicon probes, was related to stages of the oestrus cycle. By assessing neuronal responsiveness and coding precision from firing patterns and bandwidth-specific activity from local field potentials, inter-individual variance—rather than the oestrus cycle—was found to modulate visual information encoding in V1 and HPF. These findings suggest that neuronal encoding of visual stimuli is not modulated by the oestrous cycle, at least in passive viewing conditions, when the animal is not engaged in a task. Future studies should investigate neuronal encoding with other behavioural paradigms in task-specific contexts.

Lay Abstract

Plato believed that women's pre-menstrual distress was caused by the "mourning womb". Historically, case studies have reported monthly occurring symptoms in females such as intensified seizures in epileptic patients. Similarly, reproductive cycles in females from other mammalian species, such as mice and their oestrous cycle, have been found to induce changes in appetite and sociosexual behaviours. Unfortunately, such variability in behaviour and cognitive function has become a reason to exclude females from neuroscience research.

There is a large knowledge gap regarding how these cycles may affect neuronal mechanisms and activity that underlie information processing in the brain. In this study, we presented visual stimuli to female mice and assessed how neuronal activity in the brain related to oestrous cycle stages. There were no oestrous cycle-dependent changes in brain activity. Differences in brain activity were primarily due to individual variability. Such findings motivate scientists to question if the oestrous cycle impacts brain activity in specific behavioural contexts. It also encourages future studies to include females in research, whilst accounting for mouse-to-mouse variability and what aspects of individuality may be giving rise to such differences in brain activity.

1. Introduction

The female therian brain experiences fluctuations in sex hormones progesterone and oestrogen, which shape reproductive cycles such as the human menstrual and rodent oestrous cycle, respectively (Figure 1).

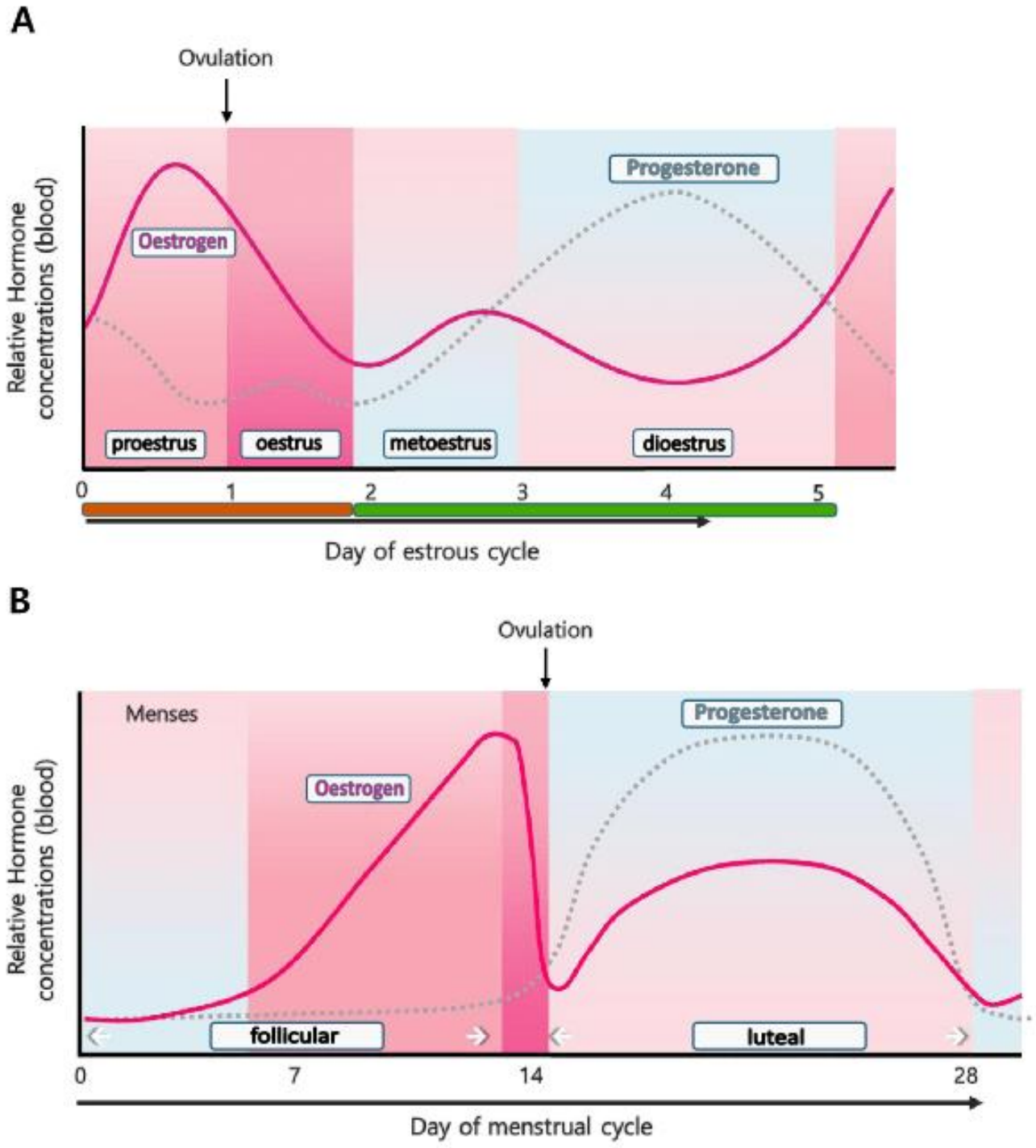

Figure 1. The Oestrous & Menstrual Cycle

(A) The oestrous cycle in female mice is a well-studied mammalian reproductive cycle, divided into four stages. Oestrogen peaks over proestrus and oestrus stages, known collectively as the 'oestrus phase' (orange bar), driving the peak of their sexual receptivity. In contrast, their sexual receptivity lowers during metoestrus and dioestrus— the 'non-oestrus phase' (green bar).
(B) The menstrual cycle in humans in their reproductive lifespan also involves a peak in oestrogen, which precedes ovulation and decreases as progesterone peaks in the latter stage, similarly to the hormonal fluctuations of the oestrous cycle. (Modified plots sourced from: Hong & Choi, 2018)

Fluctuations in behaviour have been reported to coincide with specific cycle stages. Evidence suggests that brain function involving sensory processing, notably vision, as well as learning and memory, are affected by hormonal fluctuations. Studies in menstruating humans—or "menstruators" (Rydström, 2020)—have shown increased appetite as a response to visual food cue stimuli during the luteal phase, with increased MRI-detected activity in homeostatic, reward, frontal, and visual regions of the brain (Chari et al., 2020; Bauer et al., 2017). Similarly, social interaction has been reported to change more significantly in female mice compared to males, and specifically during oestrus (Figure 1A, Chari et al., 2020). Moreover, reduced performance of female mice in spatial working memory tasks has been observed during oestrus (Rizk-Jackson et al., 2006).

Even in clinical contexts, deficits in spatiotemporal processing and object perception tasks have been reported in menstruators with Turner syndrome, whom are oestrogen deficient (Jeong et al., 2011). Symptoms of female-specific disorders such as seizure occurrences in catamenial epilepsy, experiences of visual aura (temporary disturbances in vision), as well as menstrual migraines, consistently intensified around menstruation (Herzog, 2008; Reddy, 2013; Chen, Hsu, & Chen, 2012). Performance in visual memory tasks and perceptual processing of visual cues such as faces have shown to also fluctuate with oestrogen levels throughout the menstrual cycle (Jeong et al., 2011).

Studies have presented conflicting evidence against such differences—illustrating how unclear the oestrous cycle-dependent modulation of sensory information processing is to modern science. For example, food intake has been shown to have no sex differences across 4-day oestrous cycles (Smarr, Rowland, & Zucker, 2019). Similarly, tests of anxiety, motor learning tasks, and working memory of novel object recognition concerning visual perception do not exhibit cycle changes between or within sexes in mice (Chari et al., 2020).

Yet, similarly to behavioural results, undulating changes in brain structure and neuronal signalling and the impact of the oestrous cycle on some cellular and neurophysiological-level contexts have been reported (Barth, Villringer, & Sacher, 2015). Cyclic monitoring has revealed global, not solely uterine-specific, transcriptomic changes. In addition, spine turnover and density were found to be 30% higher during proestrus compared to oestrus in cortical and hippocampal brain areas (Chen et al., 2009). Previous studies have reported changes concerning anatomy and circuitry such as increased hippocampal grey matter size during postmenstrual phases, as well as changes in progesterone-modulated functional connectivity of between the hippocampus, prefrontal cortex, and sensorimotor cortex (Pritschet et al., 2020; Protopopescu et al., 2008; Arélin et al., 2015).

Sex-dependent changes in neurophysiological functionality have been predominantly investigated in the hypothalamus and amygdala despite the possibility that information processes are altered by cyclic anatomical changes that may underly relevant neurophysiology in underexplored areas of the brain such as cortical and hippocampal regions (Micevych & Meisel, 2017). It is, thus, still unclear how the key parts of the mammalian brain—specifically cortical and hippocampal networks—regulate information processing over the progression of an oestrus cycle.

Fortunately, neuroscientists have more recently acknowledged this knowledge gap with cellular and circuit-focused studies. For example, Clemens et al.'s (2019) pioneering research investigates the impact of the oestrous cycle on cortical function (Figure 2). They present oestrogen-induced increased neuronal activity and excitability of fast-spiking GABAergic inhibitory neurons—also found in the visual cortex—expressing Esr2 (17β-oestradiol receptor) using *in vivo* and *in vitro* electrophysiological recordings of somatosensory cortical neurons in freely cycling or ovariectomised female rats in a social facial (whisker stimulation) touch paradigm. Higher spike rates were exhibited during social touch in oestrus than during non-oestrus contexts. However, it remains unclear *how* the basic sensory information processing is modulated by the oestrous cycle.

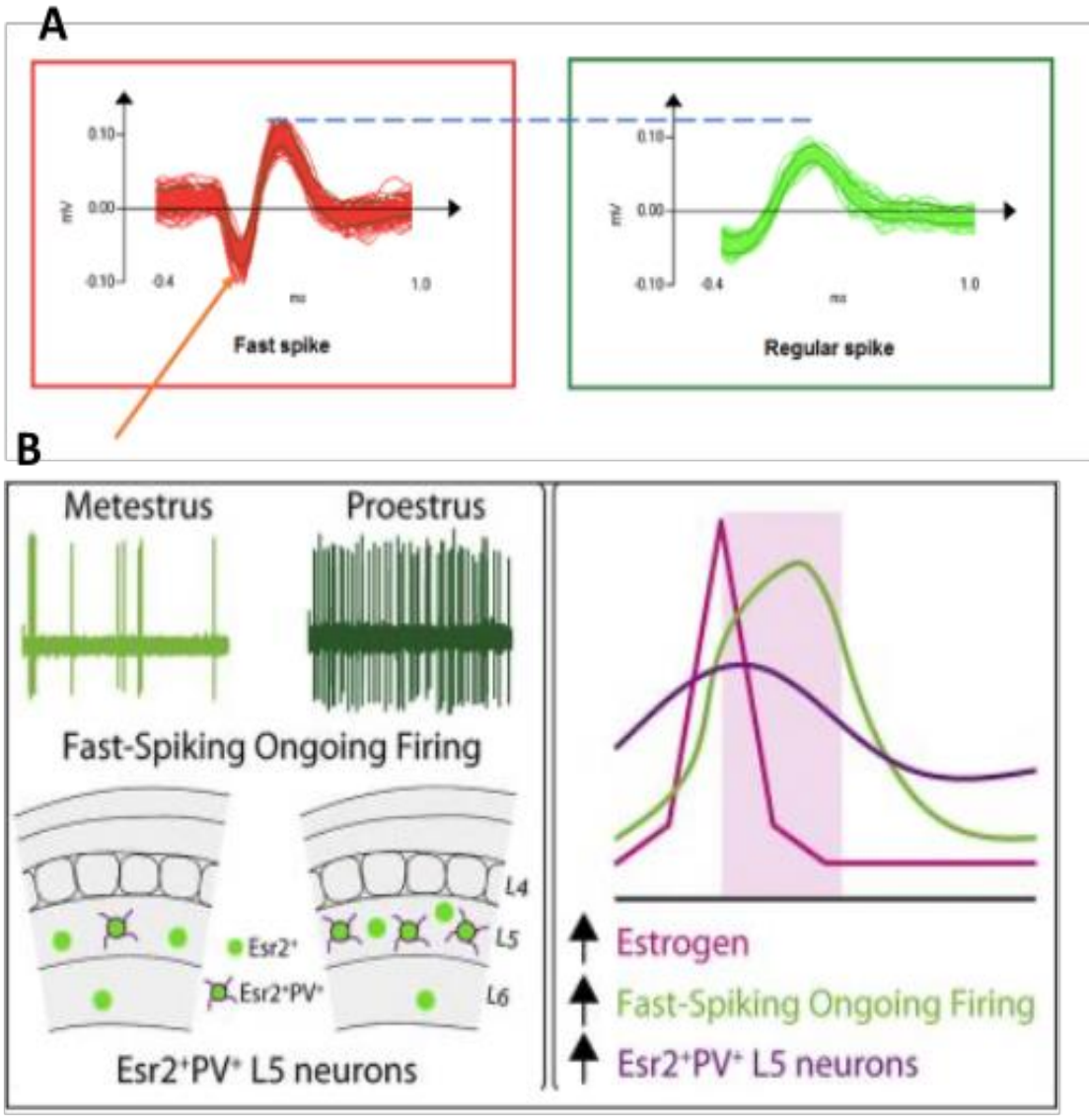

Figure 2. Somatosensory L5 Fast-Spiking Neurons Regulated by Oestrous Cycle

(A) Graphs illustrate multiple fast-spike (left) and regular-spike (right) waveforms mapped in their respective clusters, demonstrating the characteristic steep and depressive trough (marked by the orange arrow), shorter wavelength, and higher amplitude (as indicated by the blue dashed line). (Own figure, using waveform analysis images from Intech Open)

(B) Clemens et al.'s (2019) study presents a strong increase in the ongoing activity and number of $Esr2^{+}$-bearing Layer 5 parvalbumin-positive (PV^{+}) neurons during proestrus. This was found to be the same for a treatment of ovariectomised females that received oestradiol administration. This study shows the local Esr2-dependent mechanism of oestrogen in increasing fast-spiking PV+ interneuron excitability via *in vivo* and *in vitro* experiments. (Sourced from Clemens et al., 2019)

To investigate the influence of the oestrous cycle on sensory information processing, the hippocampal formation (HPF) and primary visual cortex (V1) of the female mouse are candidate circuitry models, considering, V1 anatomy and function having been extensively studied, and the common use of visually reliant and HPF-engaging behavioural experimental designs. Learning and memory, attention, and spatial information is processed in the HPF, which is reliant on and modulated by V1—vital for building internal representations of the world around us (Lee et al., 2012). It is important to investigate how neuronal processes in such indispensable brain areas are affected by the oestrous cycle and potentially give rise to sex-differences in brain function and behaviour.

2. Hypotheses & Aims

This study is based on the hypotheses that the oestrous cycle modulates visual information encoding properties in V1 and HPF, and that the activity of V1 fast-spiking neurons is enhanced during oestrus phases with more enhancement in deep V1 layers, rather than superficial V1 layers.

Thus, this study aims to understand how the oestrous cycle impacts visual stimulation encoding properties in V1 and HPF regions of female cycling mice which are performing a basic visual task—passive-viewing of visual stimuli, achieved by simultaneously conducting chronic *in vivo* large-scale electrophysiological recordings. Specifically, this study aims to gain insight on the effect of the oestrous cycle on (a) visual information encoding in V1 and HPF neuronal populations and (b) layer-specific changes in V1 fast-spiking neurons.

3. Methods

All animals and procedures concerning animals were performed under a project licence granted by the UK Home Office and compliant with the Animal (Scientific Procedures) Act 1986.

3.1 Experimental Design & Obtaining *in vivo* Electrophysiological Data

Animals & Surgery Female C57BL/6 mice aged 8-to-12 weeks were group housed in a reverse 12:12 hour light:dark cycle room with *ad libitum* access to enrichment, water, and food. Head plates were surgically implanted and the mice underwent a three-day recovery protocol of daily analgesic. Mice then underwent a craniotomy over V1 (or state coordinate) followed by a two-hour recovery period and subsequent chronic *Neuropixels* probe implantation following the protocol published by (Jun et al.,

2017; Figure 3A). After implantation, mice were housed individually but otherwise with identical conditions (Figure 3B-3C).

***Chronic Large-scale Neurophysiology Recordings with Neuropixels* Probes** *In vivo* electrophysiological activity was recorded in awake female mice (*N* = 5) using *Neuropixels* 1.0 probes (Figure 3E) in V1 and HPF. Chronic measurements using implanted *Neuropixels* probes were performed (*n* = 3, and single measurements for the remaining mice) for 10 consecutive days, with each session being 35 minutes long (Figure 3D-3E).

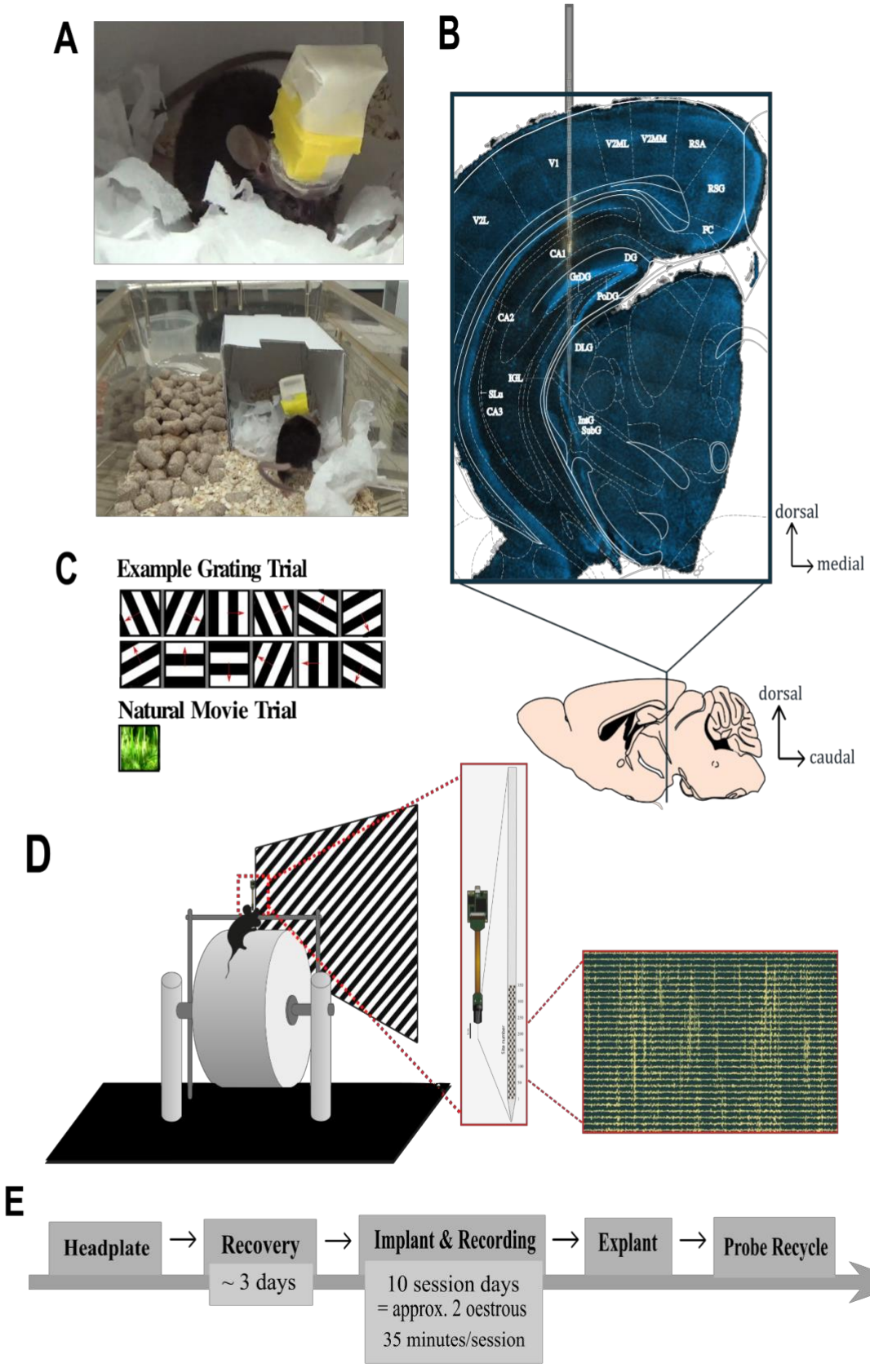
A
B
V1
V2ML
V2MM
RSA
RSG
VZL
FC
CA1
DG
GrDG
PoDG
CA2
DLG
IGL
SLu
CA3
ImG
SubG
dorsal
medial
dorsal
caudal
C
Example Grating Trial
Natural Movie Trial
D
E
Headplate
Recovery
~ 3 days
Implant & Recording
10 session days
= approx. 2 oestrous
35 minutes/session
Explant
Probe Recycle

Figure 3. Head-fixation Set-up & Chronic Neuropixels Recording Pipeline

Neuropixels 1.0 probes (Jun et al. 2017) have on-board circuitry to amplify, multiplex, and digitise voltage signals such as local field potentials (LFPs) and action potentials (APs). Signals are simultaneously recorded from 384 dual-band recording channels mapped across 960 selectable electrodes, which are tiled along a straight shank (10-mm long, 70 x 24 µm cross-sectional; boxed in red **(D)** and shown in grey **(B)**.
(A) The brain was exposed by stereotaxic craniotomy before *Neuropixels* probes were lowered into brain tissue and secured by dental cement. A connector attached to a headplate allowed for later recordings and probe stability (top). Animals lived in special cages situated next to respective home cages, with extended animal shelter and cage height to prevent damage to the fixture (bottom).
(B) Example post-hoc probe track reconstruction facilitated by staining the probe pre-implantation, of probe position V1 and HPF (insertion coordinates: Bregma medial-lateral -2.8mm, anterior-posterior -3.2mm) overlaid by Allen Brain Atlas using SHARP-Track (Rochefort Lab, 2022; Shamash et al., 2020). **(C)** Samples of drifting gratings and natural movies used (described in Section 2.1, Behavioural Paradigm). (**D)** Experimental setup with visual stimuli screen presented to the right eye of mouse situated on the fixed wheel whilst *Neuropixels* probe picks up any neuronal activity along its length as shown in the red boxes on the right. **(E)** Post-implantation, the first recording session takes place on the implant day, after which recordings take place for another 9 consecutive days.

Behavioural Paradigm **Mice were habituated to head-fixation in X minute sessions across Y days.** Electrophysiological recordings were then performed under three conditions: complete darkness and presentation of natural movies or moving gratings, during which mice were situated on a fixed wheel, in a stationary (not running) position (Figure 3E). The natural movie was a video clip of grass and leaves (60 seconds). The drifting gratings trial lasted 40 seconds, each consisting of a 12-block sequence of 2-second drifting gratings—one combination of six orientations and two directions—with a 1-second inter-block interval of a grey screen and were assigned a spatial frequency of either 0.04 or 0.16 cycle per degree. Both visual stimuli begin with a 1-second grey screen. Recordings were also done in complete darkness pre and post all visual stimulations. All visual stimuli were presented on a screen placed in front of the animal's right eye (Figure 3E).

3.2 Tracking Oestrous Cycle Stage of Female Mice

On each recording day, the oestrous stage of the animal was monitored by capturing vaginal opening photographs alongside cytologies of vaginal smears made from vaginal lavages (Figure 4).

A

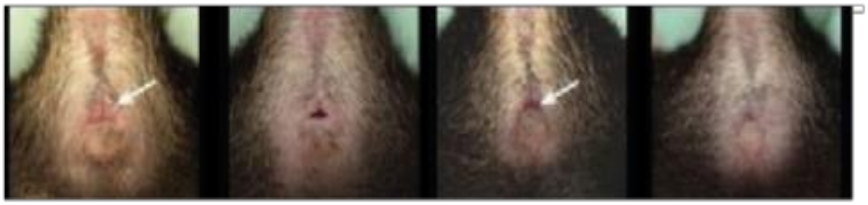

Proestrus Estrus Metestrus Diestrus

B

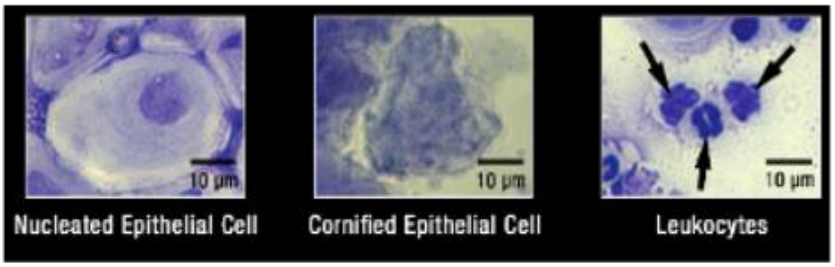

C

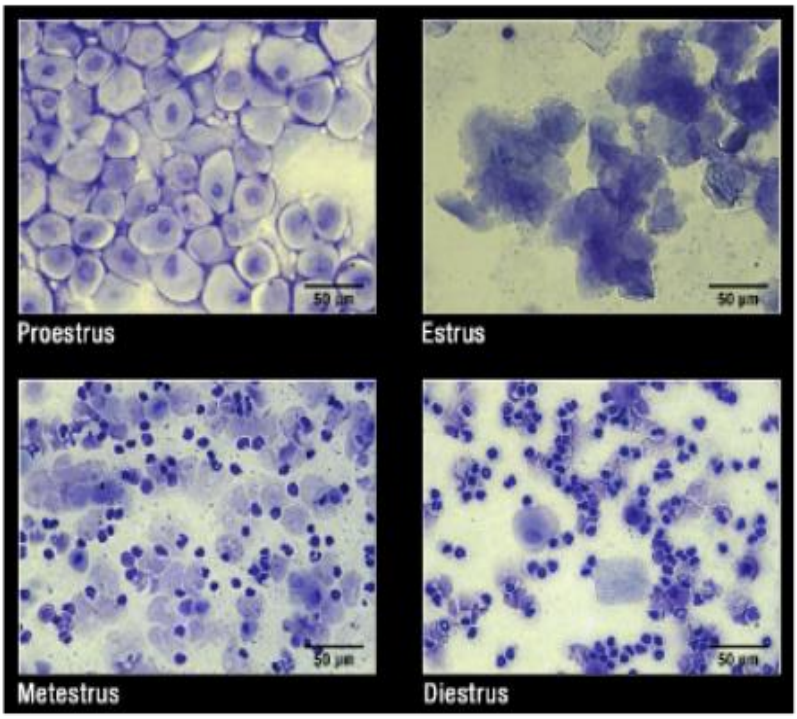

Figure 4. Monitoring Oestrous Cycle Stages in Female Mice

(A) Photographs of vaginal openings were taken prior to vaginal lavages for cycle stage evaluation based on changes in colour, moisture, and texture, by observation. White arrows indicate distinctive visual differences in shape and colour of vaginal openings when comparing proestrus and metestrus. **(B & C)** Vaginal lavages required pipette extraction (approximately three pumps of saline or distilled water, to ensure collection of vaginal wall cells) followed by immediate ejection onto glass slips, to dry on a heated blanket. Samples were stained in crystal violet (2-minute soak, with 2 1-minute rinses), before observing dried samples under a bright-field Leica microscope (FLEXA Cam C1). **(B)** Cell type morphology illustrated (horizontal lines indicates scale of 50 μm) for nucleated epithelial cells, cornified epithelial cells, and leukocytes which vary in proportion in the vaginal environment according to stage **(C)**—visual observations of which were used as a guideline to make evaluations (Ashleigh et al., 2012; See Figure 5).

Evaluations were more dependent on cytological evaluations, comparing cell type-specific morphology and proportions. An example of evaluation, using the stage-specific cytological samples as a guideline, to assess oestrous cycle stages with cytological samples magnified and photographed at x10, x20, x40 objectives using LASX software is presented in Figure 5.

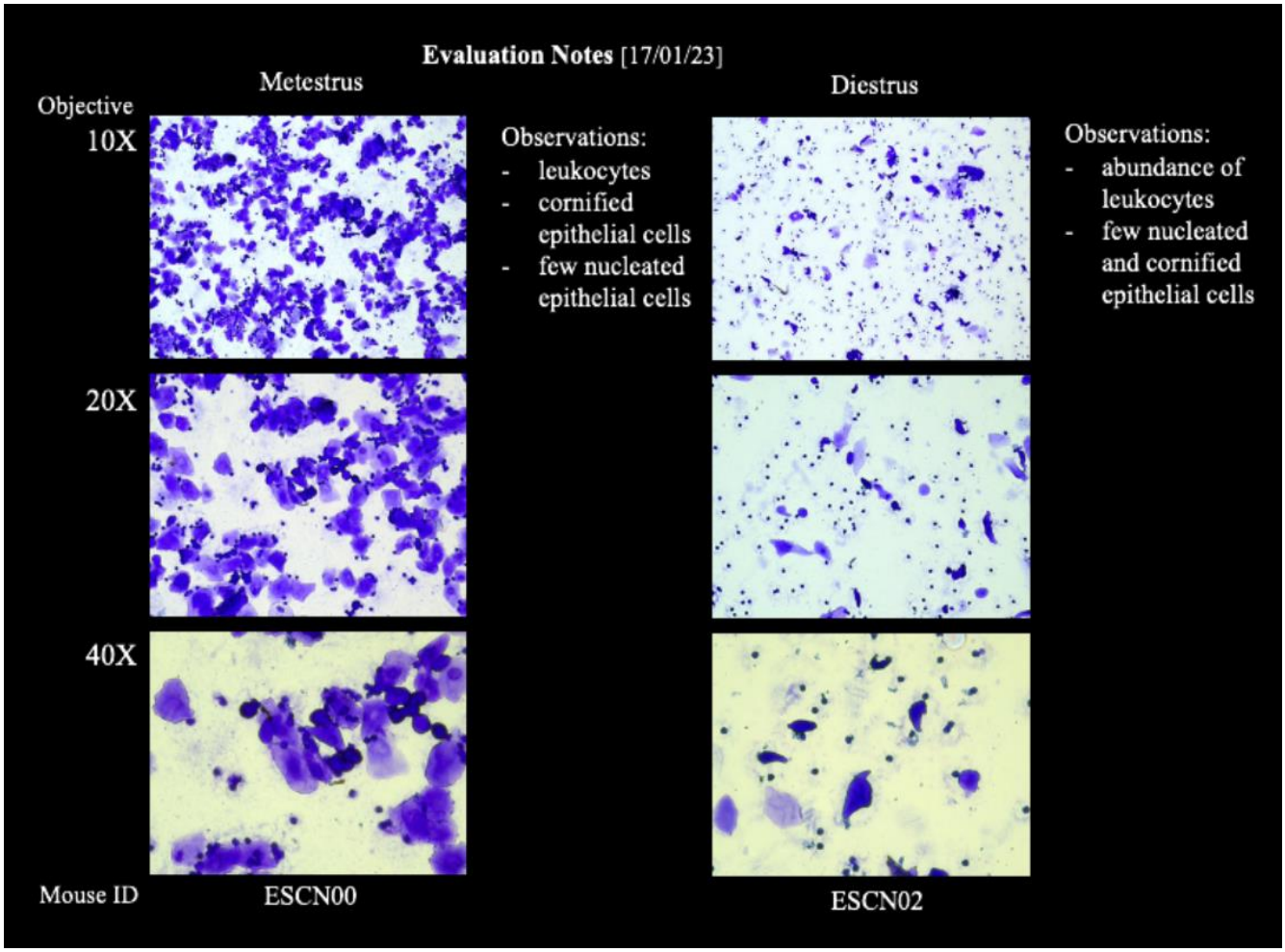

Figure 5. Example Cytological Evaluation of the Oestrous Cycle

Cytological samples from two different mice (denoted as Mouse ID) were lined up in order of lens objective strength to help determine oestrous cycle stage by observation of cell morphology, type, and abundance.

3.3 Data Analysis: Pre-processing & Post-Processing

Raw data from *Neuropixels* probes required denoising by CatGT (Bill Karsh, 2023) and spike-sorting by Kilosort 3 and spikeinterface (Pachitariu, Sridhar, & Stringer, 2023) to isolate putative neurons, and probe track reconstructions used SHARP-Track and custom Python code (Figure 6A). To identify putative fast-spiking neurons, we used a K-means algorithm to perform clustering based on spike waveform characteristics (Jia et al., 2019; Figure 6B-6C).

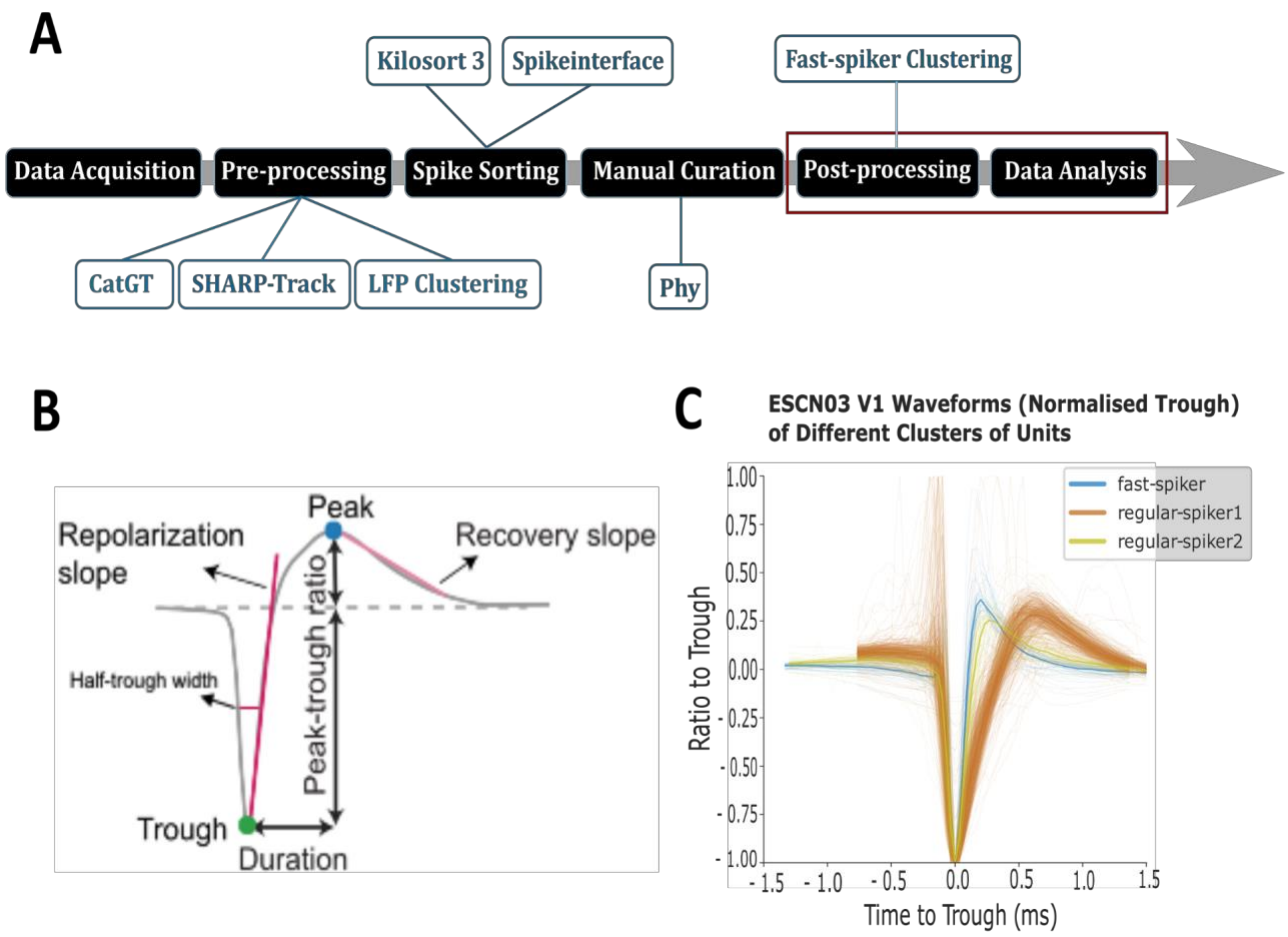

Figure 6. Data Analysis Pipeline & Identification of Putative Fast-Spiking Neurons by Clustering

(A) Data Analysis Pipeline (red box illustrates that the analysed results are the final component of this pipeline).

(B) Isolated spike waveform showing 5 quantifiable characteristics of a neuronal signal: repolarisation slope, half-trough width, trough-to-peak duration, peak-trough ratio, and recovery slope, which were used in post-processing to identify fast-spiking putative neurons according to their distinct distribution of these characteristics (Jia et al., 2019).

(C) Sample of clustered spike waveforms of example mouse based on time from trough-to-peak and peak-trough ratio. Regular-spiking neurons and fast-spiking neurons were differentiated (as colour-coded).

3.4 Data Analysis: Properties of Interest

To assess responsiveness and coding precision of visually responsive neurons, we extracted nine properties, as summarised in Table 1.

Table 1. Summary of Properties of Neuronal Coding Analysed

Properties of Neuronal Coding	
Neuron Responsivity	**Firing Rate** of Responsive Neurons
	Proportion of Responsive Neurons
Neuronal Coding Precision	**Tuning Width**
	Orientation Selectivity Index
Populational Coding Precision & Reliability	**Decoding Accuracy**
	Trial-to-trial Correlation
LFP Analysis	**Normalised Gamma Power**
	Normalised Theta Power

3.4.1 Tuning Width & Orientation Selectivity Index

The mean firing rate of neurons was used to determine the response of a neuron to each orientation from the drifting gratings and fitted with a single Gaussian curve (Figure 7A). The measured sensitivity to an orientation was plotted as a function of grating orientation to calculate a tuning curve for each neuron. Measured tuning widths were then averaged across all neurons per session (Figure 7B). The range of orientations over which a neuron responds is the tuning width, which is defined by the width of the tuning curve at half of the maximum response (Figure 7B). The narrower the tuning width, the greater the selectivity indicated for a specific orientation, as opposed to a more broad-based response.

The orientation selectivity index (OSI) measures the selectivity of a neuron to an orientation of gratings. Once the preferred orientation and orthogonal orientation have been identified, the response

of the neuron to the respective orientations is used to calculate the OSI (Figure 7B-7C). The OSI can range from 0, indicating no orientation selectivity, to 1, indicating maximal selectivity.

A

$$R(\theta) = C + R_p e \frac{-ang_{ori}(\theta - \theta_{pref})^2}{2\sigma^2}$$

B

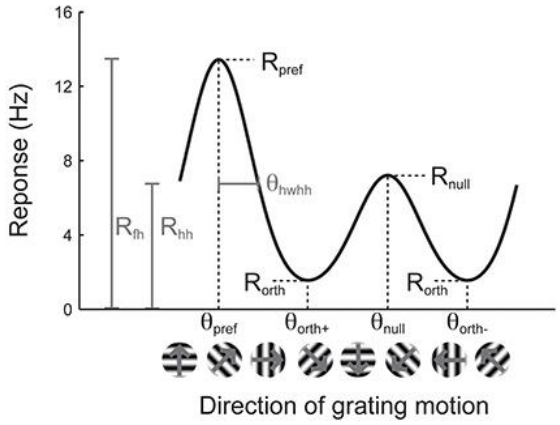

C

$$OSI = abs(\frac{\Sigma_k R(\theta_k) e^{2i\theta_k}}{\Sigma_k R(\theta_k)})$$

Figure 7. Calculating Tuning Width & OSI

(A) Equation calculating $R(\theta)$, the measured response of the neuron at a given orientation angle. C is a constant offset, R_p is the response to a preferred orientation after subtracting the offset, σ is the standard deviation of the curve, angular differences were constrained to 0-90° with the preferred orientation angle being $ang_{ori}(x) = \min(x, x - 180, x + 180)$, and θ_{pref} describes the angle of the preferred orientation. (Padamsey et al., 2022)

(B) Example plot by Mazurek et al. (2014) presenting strong tuning responses to drifting gratings in a model cell. The θ_{hwhh} describes half-width of the tuning curve at half of the maximum response height. R_{pref} is the response of the neuron to the preferred orientation—the orientation that elicits the strongest response. R_{orth} is the response to the orthogonal (perpendicular to the preferred) orientation.

(C) The OSI was determined by this equation, which is 1 minus the circular variance from the mean response to each presented orientation, as practised by Padamsey et al. (2022). Any negative values were set to zero.

Both tuning width and orientation selectivity indices were calculated for visually responsive V1 neurons and V1 putative fast-spiking neurons in both deep and superficial V1 laminae (the length of V1 was divided at 50% depth, into upper and lower halves along the *Neuropixels* probe to differentiate V1 measures as 'superficial' and 'deep'.

3.4.3 Decoding Accuracy

The accuracy of neurons in decoding visual stimulus identity was determined using a Bayesian maximum-likelihood estimator, trained to infer neuronal outputs utilising Gaussian approximation. Decoder estimations were compared with a calculated mean and corresponding standard deviation across all trials of a neuron's response spike rate to a range of grating orientations or 1-second scenes from the first 30 seconds of the movie (chance level = 1/6 and 1/30, respectively) and standard deviation. The proportion of correctly decoded stimuli was reported as the decoding accuracy, as described by Padamsey et al. (2022).

3.4.4 Trial-to-trial Correlation

Trial-to-trial correlation is a measure of the reliability of responses across multiple trials for the same stimulus or condition. A correlation coefficient was calculated across responses from each trial. The higher a trial-to-trial correlation is, the more consistently a neuron responds to a given stimulus.

3.4.5 LFP Power Analysis

In HPF, theta frequencies are observed during exploration and memory encoding whilst gamma frequencies are present during recall and long-term memory (Lisman & Jensen, 2013). The power of gamma and theta bands is normalised relative to the total power across all frequencies of a local field potential (LFP), calculated by dividing a band's power by the average power across all frequencies in a LFP signal and averaged across all recordings per session for each brain region. This measure was used to study the relative contribution of the frequency band to neuronal communication and processing.

3.5 Data Analysis: Statistical Analysis

For this preliminary study, effect sizes of results obtained for the properties investigated were calculated for future power calculations for any preceding studies.

Analysis and graphs were generated using custom code in Python3. For all statistical analyses, a significance level of $p<0.05$ was used and normality was checked using the Shapiro-Wilk test. Statistical analysis was only performed on data obtained from mice with chronic measurements and thus omitted data from animals with a discontinued single recording session.

To examine if session day influenced all properties (excluding OSI and tuning width measurements), repeated measures ANOVA (rANOVA) was used. The assumption of random sampling was met by experimental design. Mice with only one session measure were dropped from the analysis. Where assumptions of homoscedasticity and normality were not met, the non-parametric Friedman test was used.

To compare measures across different oestrous stages and between individual mice, two-way ANOVA (ANOVA), without interaction, was used. The analysis was run on all properties that rANOVA was run on, with the addition of OSI and tuning width values. In addition, one-way ANOVA (ANOVA) and one-sample t-test was used to compare overall decoding accuracy averages across neuron types and compare averages with chance level, respectively (Figure 13). Sources of pseudo replication were accounted for by averaging all measures for each mouse. All data met assumptions for statistical analysis.

4. Results

4.1 Spontaneous activity and neuronal responsiveness to visual stimuli is unaffected by oestrous cycle progression.

To examine the effect of the oestrous cycle on neuronal responsiveness, firing rates were examined across cycle stages.

Firing rates were consistently higher during proestrus and metestrus stages, in grating and movie responsive V1 neurons, irrespective of neuron type. For instance, average firing rates in V1 fast-spiking movie-responsive neurons were approximately 1.7 times higher during metestrus (M = 7.79, SD = 4.24) than dioestrus (M = 4.65, SD = 1.36). However, two-way ANOVA revealed that the effect of cycle stages on firing rates were nonsignificant for both grating and movie-responsive neurons, regardless of visual stimuli or putative neuron type (See Figure 8 legend; $p > 0.05$). In addition, there was no significant variation between firing rates of different mice identities within each stage (Figure 8; $p > 0.05$).

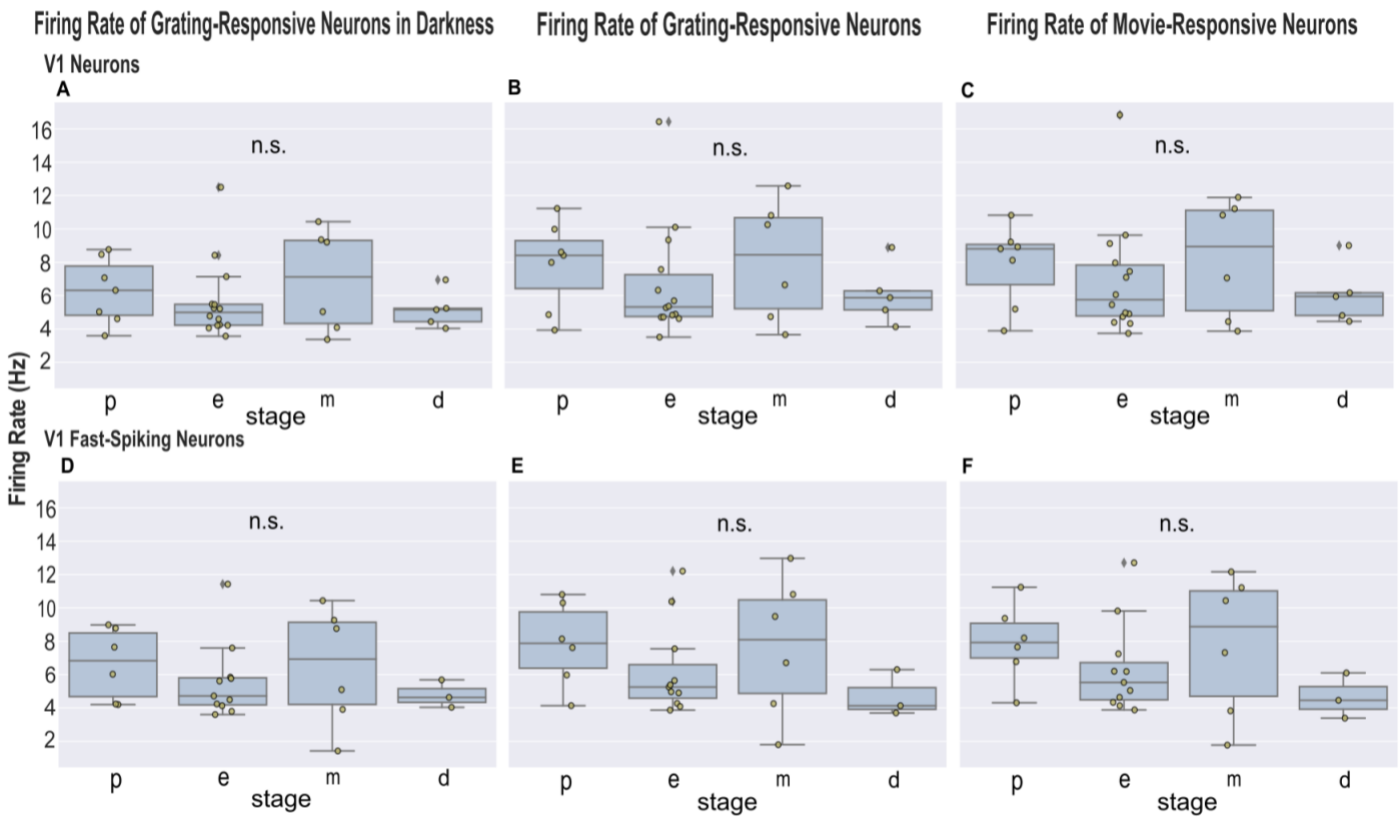

Figure 8. Firing Rates of Female Mouse V1 Neurons & Fast-Spiking Units Across Oestrous Cycle Stages During Passive-Viewing of Visual Stimuli

Boxplots showing overall averages of firing rates calculated from each mouse (n = 3) across oestrous cycle stages, proestrus (p), oestrus (e), metestrus (m), and dioestrus (d), for putative V1 regular-spiking and fast-spiking neurons. **(A - F)** Comparison of average firing rates of V1 grating-responsive neurons in darkness and grating and movie-responsive neurons during passive-viewing treatments did not present a statistically significant effect of stage on firing rates (F(3, 6) = 0.61, p = 0.63; F(3,6) = 1.07, p = 0.43; F(3,5) = 0.54, p = 0.67) and similarly for fast-spiking neurons under the same treatments (F(3, 5) = 0.58, p = 0.65; F(3,5) = 0.68, p = 0.60; F(3, 5) = 0.75, p = 0.57). Each dot represents individual measurements. The effect of mouse identity on firing rates were also statistically non-significant for grating and movie-responsive regular and fast-spiking neurons under dark and visual treatments **(A - F:** F(2, 6) = 0.02, p = 0.98; F(2,6) = 0.91, p = 0.45; F(2,6) = 0.65, p = 0.56; F(2,5) = 0.90, p = 0.46; F(2,5) = 2.50, p = 0.18; F(2,5) = 1.36, p = 0.34**)**.

4.2 The proportion of visually responsive neurons was stable throughout sessions and across oestrous stages.

To examine if proportion fluctuates with the oestrous cycle, proportion of responsive neurons in the V1 and HPF were compared over session days and stages.

Figure 9. Proportion of Responsive Neurons in V1 & HPF

Line plots **(A - C)** illustrate the proportion of stimulus-responsive neurons recorded over 10 consecutive sessions (1 session/day) from each mouse (N = 5 as denoted by Mouse ID (identification); n = 3 for statistical testing). Repeated measures were compared over session days and were statistically non-significant for V1 grating-responsive, movie-responsive, and HPF movie-responsive neurons, respectively ($X^2(9) = 7.93$, $p = 0.54$; $F(9,18) = 1.59$, $p = 0.19$; $X^2(9) = 13.74$, $p = 0.13$). **(D - F)** Boxplots comparing overall averages of proportions calculated from each mouse (n = 3) across oestrous cycle stages. Each dot represents individual measurements.

There was no statistically significant difference in proportion between session days ($p > 0.05$), indicating good quality and stable chronic recording conditions across days. In addition, averaged proportions of V1 movie and grating-responsive neurons across oestrous cycle stages were statistically non-significant ($F(3,6) = 0.989$, $p = 0.459$; $F(3,6) = 0.835$, $p = 0.522$). There was no detectable effect of mouse identity on proportions for both stimuli within stages ($F(2,6) = 2.43$, $p = 0.17$; $F(2,6) = 1.59$, $p = 0.28$, Figure 9).

Similarly, there was no significant difference in proportions of HPF movie-responsive neurons between stages ($F(3,2) = 0.43$, $p = 0.74$). However, there was a statistically significant effect of mouse identity on the proportion of movie-responsive neurons within stages ($p = 0.034$).

4.3 Orientation selectivities and tuning widths of V1 grating-responsive and fast-spiking neurons were stable across oestrous cycle stages.

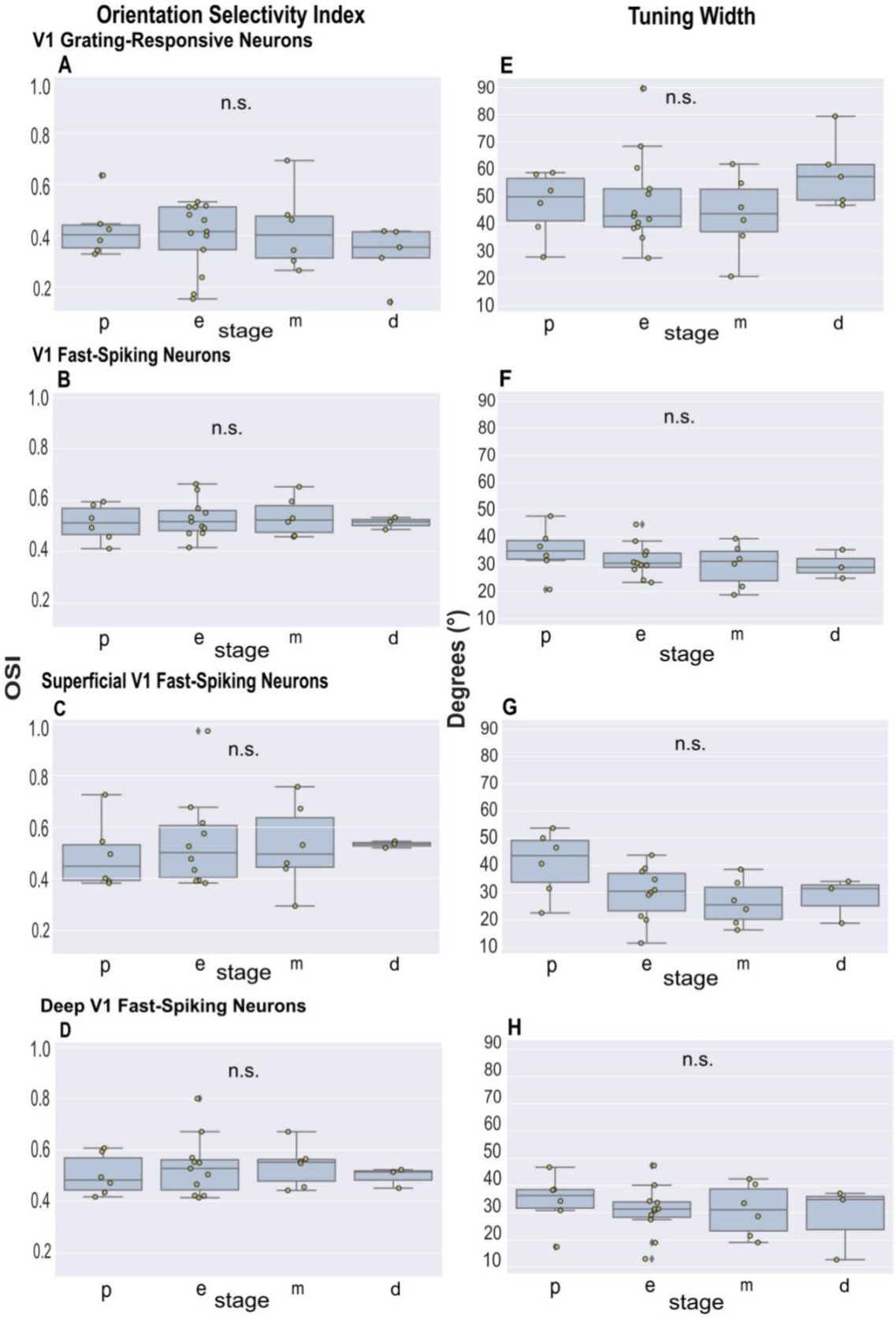

Figure 10. Averaged Tuning Width and OSI for V1 Grating-Responsive Neurons & V1 Grating-Responsive Fast-Spiking Neurons

Presented in boxplots **(A - H)**, V1 grating-responsive, fast-spiking neurons, and superficial and deep layer-specific fast-spiking neurons did not present statistically significant differences when average OSIs (**A - D**: $F(3, 5) = 0.75$, $p = 0.57$; $F(3, 5) = 0.53$, $p = 0.68$; $F(3, 5) = 0.21$, $p = 0.89$; $F(3, 5) = 0.94$, $p = 0.49$) and tuning widths (**E - H**: $F(3, 6) = 0.03$, $p = 0.99$; $F(3, 5) = 0.16$, $p = 0.92$; $F(3, 5) = 0.19$, $p = 0.90$; $F(3, 5) = 0.69$, $p = 0.59$) were compared across stages. Each dot represents individual measurements. The effect of mouse identity on OSI of V1 fast-spiking neurons, regardless of laminar depth, were also statistically non-significant (**B - D:** $F(2, 5) = 4.22$, $p = 0.08$; $F(2,5) = 1.45$, $p = 0.32$; $F(2,5) = 3.37$, $p = 0.12$) and tuning width of V1 superficial and deep fast-spiking neurons (**G, H:** $F(2,5) = 3.11$, $p = 0.13$; $F(2,5) = 4.91$, $p = 0.07$). However, mouse identity proved to have a statistically significant effect on OSI and tuning width of V1 grating-responsive neurons (**A, E**: $F(2,6) = 12.00$, $p = 0.008$; $F(2,5) = 15.99$, $p = 0.004$), as well as on tuning width of V1 fast-spiking neurons (**F**: $F(2,5) = 6.48$, $p = 0.04$).

The visual response selectivity to stimulus orientation was assessed by two measures: the orientation selectivity index (OSI) and the tuning width of orientation tuning curves based on the response firing rates to 8 oriented drifting gratings. OSIs and tuning widths were compared over session days and stages to investigate any oestrous-cycle-dependent modulation of selectivity. No statistical difference over session days or stages were reported (Figure 10A-10H). However, mouse identity has a statistically significant effect on OSI and tuning width of V1 grating-responsive neurons (Figure 10A, 10E: $F(2,6) = 12.00$, $p = 0.008$; $F(2,5) = 15.99$, $p = 0.004$), as well as on tuning width of V1 fast-spiking neurons (Figure 10F: $F(2,5) = 6.48$, $p = 0.04$). Overall, OSIs and tuning widths were consistent over the oestrous cycle, regardless of putative neuron type and laminar depth.

4.4 Neuronal population coding precision and reliability of V1 neuron responses exhibited no cyclic changes throughout the oestrous cycle.

The decoding accuracy of visual stimuli as well as the reliability of neuronal responses and trial-to-trial correlation of neuronal responses to natural stimuli (movie of grass) was compared over session days and stages.

Decoding accuracies were higher in V1 grating and movie-responsive neurons across session days than chance level (0.16 and 0.03 respectively; Figure 11A-11D). Comparison between decoding accuracies over session days did not present any statistically significant differences for V1 grating and

movie-responsive neurons. Aligning with these findings, this property was consistent over oestrous stages for both grating and movie-responsive neurons ($F(3,6) = 0.98$, $p = 0.46$; $F(3,6) = 1.10$, $p = 0.42$). Mouse identity, however, had a statistically significant effect on decoding accuracy of both V1 grating and movie-responsive neurons ($F(2,6) = 8.93$, $p = 0.02$; $F(2,6) = 12.97$, $p = 0.007$, Figure 11).

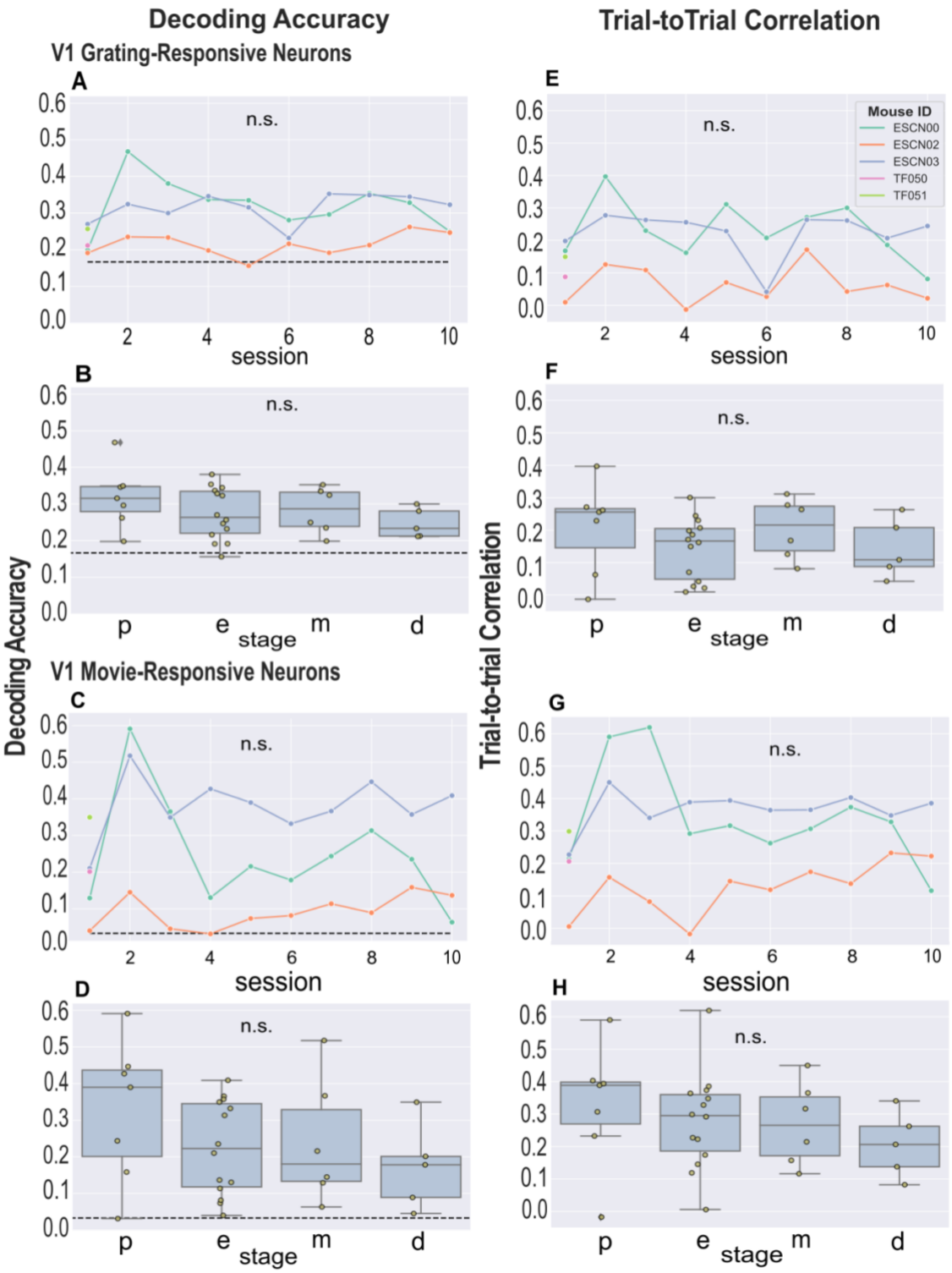

Figure 11. Decoding Accuracy and Trial-to-trial Correlation in V1 Neurons

Presented as line plots, differences between decoding accuracies calculated over session days, did not meet statistical significance for **(A)** V1 movie ($F(9, 18) = 2.47$, $p = 0.051$) and **(C)** grating-responsive neurons ($F(9, 18) = 1.798$, $p = 0.138$). **(E & G)** Test results for by-session day comparison of trial-to-trial correlation and **(B & D)** decoding accuracy and **(F & H)** trial-to-trial correlation by-stage comparisons, illustrated as boxplots, were reported in Results Section 4.4. Each dot represents a single measurement. Dashed lines represent chance level accuracies—0.16 and 0.33—for grating and movie responsive neurons respectively.

The effect of session days on trial-to-trial correlation of V1 grating-responsive neurons was indicated to be statistically significant ($X^2(9) = 20.31$, $p = 0.02$; Figure 11E). However, averaged trial-to-trial correlation for grating-responsive neurons did not differ across stages ($F(3,6) = 0.47$, $p = 0.71$; Figure 11F).

There was no statistically significant effect of session days or oestrous cycle stage on trial-to-trial correlation of V1 movie-responsive neurons ($F(9,18) = 1.43$, $p = 0.25$; $F(3,6) = 0.67$, $p = 0.60$; Figure 11G, 11H). Mouse identity was found to have a statistically significant effect on this property within stages for both grating and movie-responsive neurons ($F(2,6) = 11.21$, $p = 0.01$; $F(2,6) = 12.63$, $p = 0.01$).

4.5 HPF movie-responsive neurons exhibited a stable response to visual stimuli across the oestrous cycle.

Comparison of HPF movie-responsive neuron firing rate measures did not differ significantly across sessions ($F(9,18) = 2.47$, $p = 0.06$), which was also reported for decoding accuracy and trial-to-trial correlation measures ($X^2(9) = 6.66$, $p = 0.67$; $F(9,18) = 0.59$, $p = 0.79$; Figure 12A, 12C, 12E).

Similarly, there was no significant effect of cycle stage on measures of firing rate, decoding accuracy, and trial-to-trial correlation ($F(3,6) = 0.28$, $p = 0.84$; $F(3,6) = 0.62$, $p = 0.63$; $F(3,6) = 1.45$, $p = 0.32$; Figure 12B, 12D, 12F). Mouse identity also did not have an effect on the same properties ($F(2,6) = 2.69$, $p = 0.15$; $F(2,6) = 0.82$, $p = 0.49$; $F(2,6) = 1.67$, $p = 0.26$, respectively).

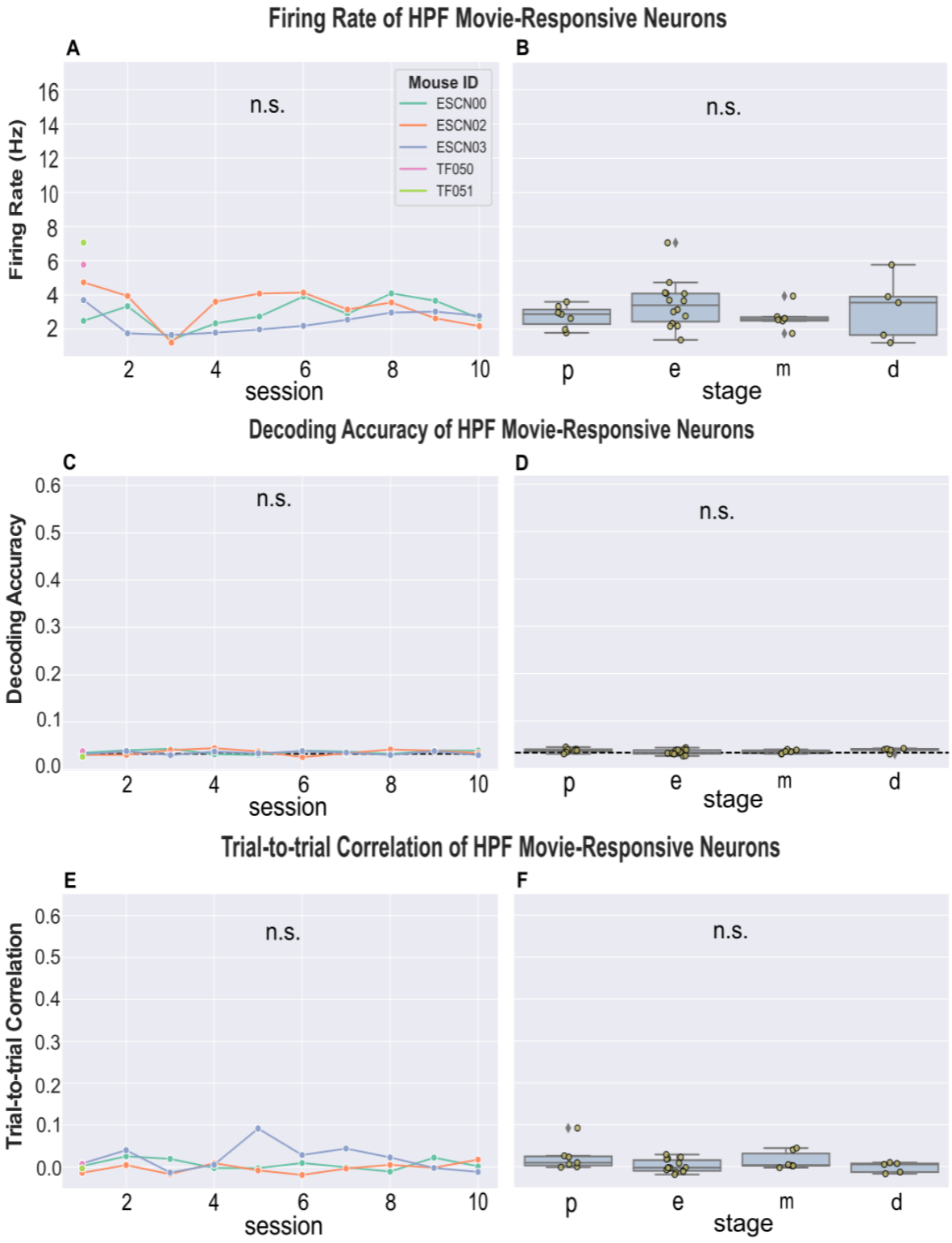

Figure 12. Measured Firing Rate, Decoding Accuracy, & Trial-to-Trial Correlation of HPF Movie-Responsive Neurons

Line plots **(A, C, E)** show firing rate, decoding accuracy, and trial-to-trial correlation measures over 10 session days for each mouse (*N* = 5). **(B, D, F)** Adjacent boxplots show firing rate, decoding accuracy, and trial-to-trial correlation measures, respectively averaged across stages. Each dot represents a single measurement. The dashed black line indicates chance level accuracy for movie-responsive neurons at 0.033. There were no measures of significant effect of session days or oestrous cycle stage on any of the properties, nor was there an effect of mouse identity on the measures.

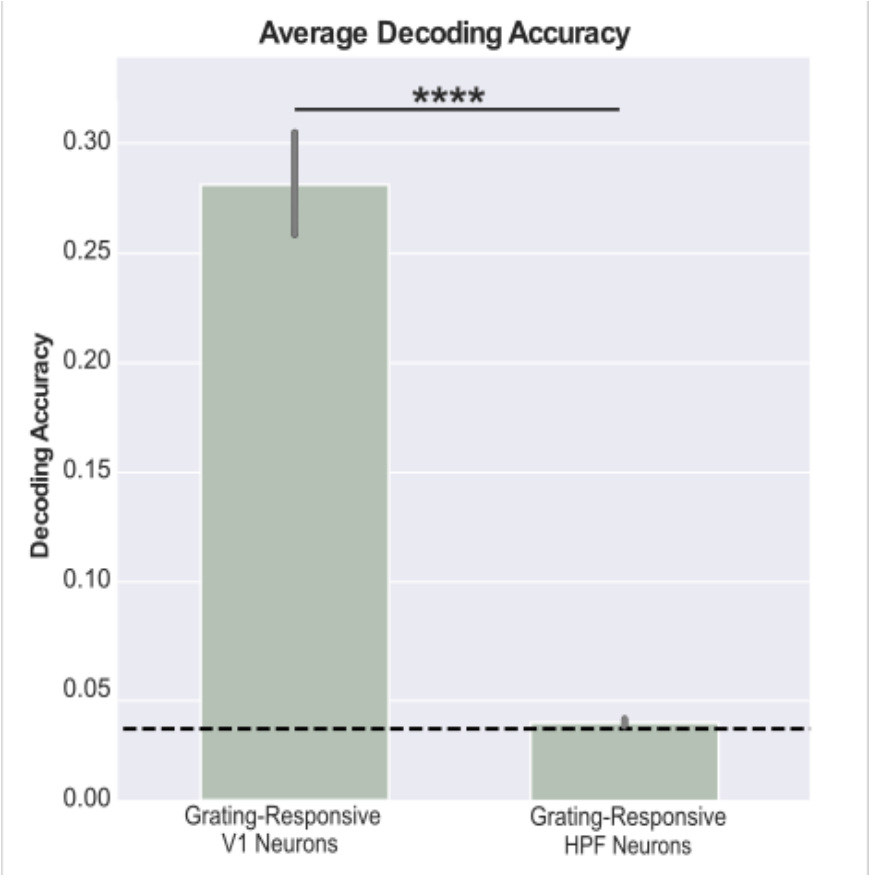

Figure 13. Comparison of Average Decoding Accuracies V1 & HPF Neurons

Average decoding accuracies, presented as a bar graph, were calculated from all V1 and HPF grating-responsive neurons across 10 sessions in 5 mice. The black dashed line represents the chance level at 0.033. T-test comparison of the two averages indicated statistical significance ($p < 0.0001$, as denoted ****).

To compare coding precision in V1 and HPF neurons, average decoding accuracies were calculated (Figure 13). The average decoding accuracy of HPF grating-responsive neurons ($M = 0.036$, $SD = 0.005$) was found to be significantly lower than the average decoding accuracy of V1 grating-responsive neurons ($M = 0.283$, $SD = 0.07$, $t(29) = -19.85$, $p < 0.001$; Figure 13).

4.4 Gamma & theta bands of HPF LFP activity are stable across oestrous cycle stages.

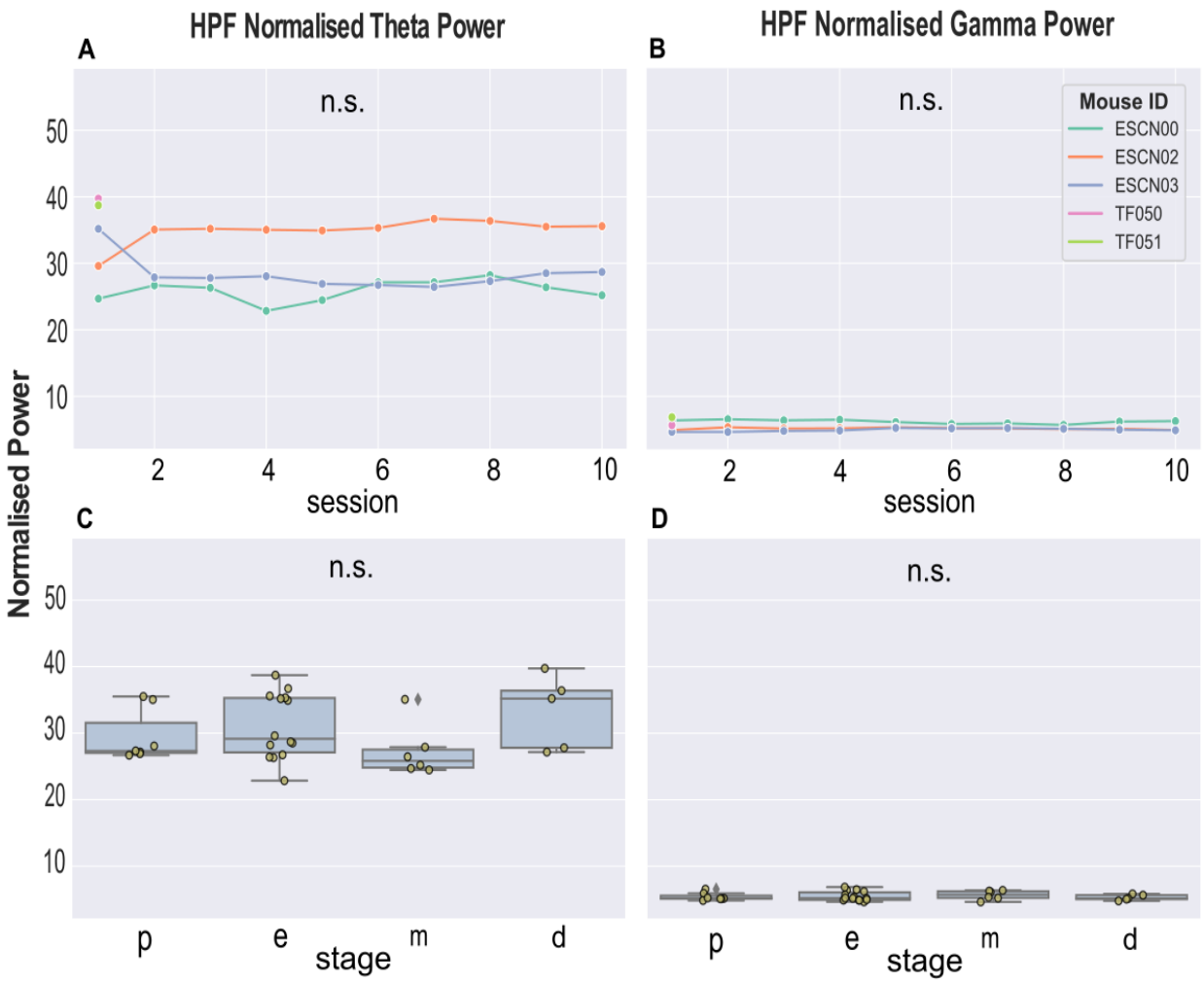

Figure 14. HPF Normalised Gamma & Theta Power Across Sessions & Oestrous Cycle Stages

Normalised theta and gamma power measures presented as line plots **(A & B)** over session days for each mouse (*N* = 5). **(C & D)** To compare across stages, normalised theta and gamma power were respectively averaged, illustrated here as boxplots. Each dot represents a single measurement.

HPF LFP activity was analysed to investigate normalised gamma and theta power and whether it fluctuates over session days and cycle stages. There were no statistically significant differences in normalised theta and gamma power across sessions ($X^2(9) = 7.95$, $p = 0.54$; $F(9,18) = 0.37$, $p = 0.94$; Figure 14A & 14B) or stage ($F(3,6) = 0.90$, $p = 0.49$; $F(3,6) = 3.89$, $p = 0.07$; Figure 14C & 14D). These results indicate the high consistency of chronic recordings across the 10 sessions for each

individual mouse. However, there was a statistically significant effect of mouse identity on both normalised theta and gamma power measures ($F(2,6) = 89.22$, $p < 0.001$; $F(2,6) = 148.39$, $p < 0.001$).

4.5 Effect sizes of preliminary results vary according to the property measured.

Results of this preliminary study were examined for their respective effect sizes as a reference for relevant power analyses in future studies. Effect sizes were shown to vary, depending on the neural encoding properties that were investigated, as illustrated in Table 2.

Table 2. Effect Sizes

Neuronal Encoding Property	Effect Size
Proportion of V1 Movie-Responsive Neurons	0.331
Proportion of HPF Movie-Responsive Neurons	0.178
Firing Rate of V1 Movie-Responsive Neurons	0.213
Firing Rate of HPF Movie-Responsive Neurons	0.123
Firing Rate of V1 Fast-Spiking Movie-Responsive Neurons	0.309
OSI V1 Grating-Responsive Neurons	0.042
OSI V1 Fast-Spiking Neurons	0.241
Decoding Accuracy V1 Movie-Responsive Neurons	0.355
Decoding Accuracy V1 Grating-Responsive Neurons	0.328
Decoding Accuracy HPF Movie-Responsive Neurons	0.237
Normalised Gamma Power HPF Neurons	0.661

Summary of effect sizes calculated from a selection of preliminary results of properties investigated. The neuron putative type that the property measures were obtained from are detailed next to the property in bold.

5. Discussion

4.1 Absence of oestrous cycle-dependent modulation of visual information encoding.

The results consistently present no fluctuant effect of oestrous cycle on visual information encoding.

Firing Rate & Proportion of Responsive Neurons Consistency in firing rates indicate that V1 and HPF neuronal excitability is not modulated by the oestrous cycle under passive-viewing contexts. Similarly, the proportion of both grating and movie-responsive neurons within the total number of recorded neurons were consistent over oestrous cycles and stages. This infers that any variability observed in firing rate and other neuronal encoding properties were likely to not have been caused by differences in the number of responsive neurons recorded at each session day or stage in both V1 and HPF.

Selectivity OSI and tuning width were consistent over the oestrous cycle, suggesting that selectivity of neurons to specific visual stimuli and the range of stimuli to which a neuron is responsive to is unaffected by sex-hormone fluctuations, irrespective of the fast-spiking neuron laminar depth.

Trial-to-trial Correlation Consistency of trial-to-trial correlation indicates high reliability of recorded activity over sessions and stages, which suggests that the stability observed across selectivity, firing rates, decoding accuracies, and LFP analysis can be trusted.

Decoding Accuracy Consistency of decoding accuracies across sessions and stages show that accuracy of neuronal activity in encoding a visual stimulus is high but not modulated by the oestrous cycle in V1 neurons. In addition, HPF neurons do not encode passively viewed visual stimuli information as well as V1 neurons do. V1 neuron decoding accuracy was higher than chance level for both movie and grating trials in comparison to HPF neurons, which were comparatively not as responsive as V1 neurons.

LFP Analysis Consistency in HPF LFP analysis indicates that neural population activity, which had higher normalised theta power than gamma, does not fluctuate with the oestrous cycle during passive-viewing contexts.

4.2 Inter-individual variability marks a more prominent effect on visual information encoding than the oestrous cycle.

These results suggest a higher prominence of inter-individual variability than oestrous cycle-dependent variability in neuronal activity. This finding is resonant with Levy et al.'s paper (2023) in which they characterise the spontaneous open-field behaviour of female and male mice whilst monitoring the oestrous cycle in females. Negligible effects of the cycle stages were found on female behaviour, whilst unique characteristics of exploration were exhibited in each mouse. Interestingly, this inter-individual variability as well as intra-individual variability was smaller than that of male behaviour. Together, these findings provide empirical support to practise inclusion of both sexes for experiments querying spontaneous visual activity and as well as spontaneous behaviours.

4.3 Study Limitations

Firstly, as this study focused solely on passive viewing tasks, results were obtained for only one type of behavioural task. Second, as a preliminary study, the experimental design, analysis, and variability in effect sizes would benefit from a higher sample size of both mice count and recorded neuron count. In addition, as single *Neuropixels* probes were used per recording session, it is also possible that sample size of responsive neurons recorded was not maximised, simply due to the location of insertion in V1 (i.e., how anterior or posterior the probe was within the retinotopy of V1), affecting the proportion of neurons responsive to the visual stimuli used and consequently, the neuronal responses measured.

In addition, oestrous cycle stages may have not been evaluated correctly. Although vaginal and cytological photographs were revised and compared to correct inaccurate evaluations, it is possible that some incorrect evaluations were missed due to photo quality as well as the possibility of unconscious bias in choosing the cytological sample area to photograph and in deciding which stage a mouse belonged to due to a mouse being in the transition period between two stages.

4.4 Future Directions: Potential Preceding Study Experimental Design

Despite HPF neurons previously been found to fluctuate in increased dendritic turnover and excitability with reproductive cycles, no changes were observed functionally, with a lack of decoding accuracies upon visual stimulation. With other studies showing activity corresponding with visual stimuli in a non-passive behavioural paradigm, this finding is most likely due to a lack of HPF engagement. To address

the limitation of this study being passive-viewing exclusive, chronic *in vivo* electrophysiological recordings of V1 and HPF in awake and cycling female mice on a non-fixed wheel, in, for instance, a virtual-reality spatial navigation task, could be implemented as a further experiment to engage the hippocampus and examine differences in neuronal excitability and effect of oestrous-dependent modulation on that activity.

Neuropixels 2.0 probes, each consisting of 4 shanks, could be used to increase breadth of regions recorded across V1, with 4 shanks, as well as the number of neurons recorded simultaneously to increase the sample size. Prior to recording, the study would benefit from mapping the retinotopy of V1 to ensure that neurons recorded are those responsive to the visual stimuli presented.

Given the rapidly changing hormonal profile throughout the four-day oestrous cycle, a more accurate oestrous cycle tracking system that reduces levels of human bias in determining a specific stage would benefit research by generating reliable results. For instance, Wolcott et al. (2022) utilised deep learning to determine oestrous stages in rodents with automated classification. Their procedure is flexible across strains, rodent species, as well as cytological stains, and would prevent human bias whilst providing time-efficiency (Wolcott et al., 2022).

4.4 Future Directions: Reporting Sex & Implications of Outcomes

Historically, there has been a lack in reporting sex in published papers, in neuroscience and across other disciplines excluding reproductive biology (Beery & Zucker, 2010). Regardless of the behavioural paradigm used, sex of the employed experimental model should be constantly documented in preceding studies, universally. This benefits future meta-analyses that can refer to available data to facilitate piecing together an accurate representation of the neuronal mechanisms involved in oestrous cycle-dependent modulation of behavioural and brain function.

Reporting sex is also informative in situations where the same outward behavioural response is mediated by different brain mechanisms. With some behavioural experiments testing for, for instance, anxiety, being originally established and run on a male-centric cohort, basic research in female psychiatry and animal testing must establish a valid and standardised experimental protocol for female animals, adjusting such protocol based on whether the same behaviour is elicited with sex-specific brain mechanisms and affected by various confounding factors (Lovick et al., 2021).

Documentation of sex is integral for clinically relevant studies, not solely to prove sex differences, but to gain a better understanding of how sex may influence the experimental design, analysis, reproducibility, and relevance of the research performed (Brooks & Clayton, 2017).

Females have also been excluded from cohorts to prevent the assumed sex-induced variability (Beery & Zucker, 2001; Chari et al., 2020). Interestingly, variability in data categorised by behavioural traits and obtained as neurochemical, histological, or electrophysiological measures was not higher in females in comparison to that of males (Becker, Prendergast, & Liang, 2016). This preliminary study tested the main hypothesis that there would be oestrous-cycle-dependent modulation of brain function, observed in the form of variability across stages in mouse V1 and HPF electrophysiology data. If results presented oestrous-dependent modulation, there would be less variability among mice and a consistent cyclic pattern of variation across stages in the neuronal activity recorded, encouraging experimental designs to account for the possibility of oestrous cycle-induced variability. However, the data support the contrary, with high variability among mice and no cyclic pattern of variation across stages in recorded data, suggesting no oestrous-dependent modulation.

The negative results in variability throughout this preliminary study support the inclusion of female cohorts without the concern of oestrous-cycle-induced variability and encourage investigating how inter-individual variability may be accounted for in future studies.

5. Conclusion

This preliminary study consistently presented no oestrous cycle-dependent modulation of V1 and HPF activity and prominent inter-individual variability across visual stimulation encoding properties. There is still more to be understood around sex-dependent changes in brain function and sex-differences in general, such as cyclic symptoms correlated with menstruation that debilitate quality of life in female-specific neuropsychiatric disorders. Research should be directed in a way to minimise this gap in knowledge and investigate sex-specific differences but whilst reckoning individuality, regardless of sex.

6. References

Arélin, K. *et al.* (2015) 'Progesterone mediates brain functional connectivity changes during the menstrual cycle—a pilot resting state MRI study', *Frontiers in Neuroscience*, 9. Available at: https://doi.org/10.3389/fnins.2015.00044.

Arnoni-Bauer, Y. *et al.* (2017) 'Is It Me or My Hormones? Neuroendocrine Activation Profiles to Visual Food Stimuli Across the Menstrual Cycle', *The Journal of Clinical Endocrinology & Metabolism*, 102(9), pp. 3406–3414. Available at: https://doi.org/10.1210/jc.2016-3921.

Barth, C., Villringer, A. and Sacher, J. (2015) 'Sex hormones affect neurotransmitters and shape the adult female brain during hormonal transition periods', *Frontiers in Neuroscience*, 9. Available at: https://doi.org/10.3389/fnins.2015.00037.

Becker, J.B., Prendergast, B.J. and Liang, J.W. (2016) 'Female rats are not more variable than male rats: a meta-analysis of neuroscience studies', *Biology of Sex Differences*, 7(1), p. 34. Available at: https://doi.org/10.1186/s13293-016-0087-5.

Beery, A.K. and Zucker, I. (2011) 'Sex bias in neuroscience and biomedical research', *Neuroscience & Biobehavioral Reviews*, 35(3), pp. 565–572. Available at: https://doi.org/10.1016/j.neubiorev.2010.07.002.

Brooks, C.E. and Clayton, J.A. (2017) 'Sex/gender influences on the nervous system: Basic steps toward clinical progress: Basic Steps to Clinical Progress', *Journal of Neuroscience Research*, 95(1–2), pp. 14–16. Available at: https://doi.org/10.1002/jnr.23902.

Chari, T. *et al.* (2020) 'The Stage of the Estrus Cycle Is Critical for Interpretation of Female Mouse Social Interaction Behavior', *Frontiers in Behavioral Neuroscience*, 14, p. 113. Available at: https://doi.org/10.3389/fnbeh.2020.00113.

Chen, J.-J., Hsu, Y.-C. and Chen, D.-L. (2012) 'Pure menstrual migraine with sensory aura: a case report', *The Journal of Headache and Pain*, 13(5), pp. 431–433. Available at: https://doi.org/10.1007/s10194-012-0450-9.

Chen, J.-R. *et al.* (2009) 'Gonadal Hormones Modulate the Dendritic Spine Densities of Primary Cortical Pyramidal Neurons in Adult Female Rat', *Cerebral Cortex*, 19(11), pp. 2719–2727. Available at: https://doi.org/10.1093/cercor/bhp048.

Clemens, A.M. *et al.* (2019) 'Estrus-Cycle Regulation of Cortical Inhibition', *Current Biology*, 29(4), pp. 605-615.e6. Available at: https://doi.org/10.1016/j.cub.2019.01.045.

Herzog, A.G. (2008) 'Catamenial epilepsy: Definition, prevalence pathophysiology and treatment', *Seizure*, 17(2), pp. 151–159. Available at: https://doi.org/10.1016/j.seizure.2007.11.014.

Inoue, S. (2022) 'Neural basis for estrous cycle-dependent control of female behaviors', *Neuroscience Research*, 176, pp. 1–8. Available at: https://doi.org/10.1016/j.neures.2021.07.001.

Jeong, J.-K. *et al.* (2011) 'The Mouse Primary Visual Cortex Is a Site of Production and Sensitivity to Estrogens', *PLoS ONE*. Edited by I.A. Hansen, 6(5), p. e20400. Available at: https://doi.org/10.1371/journal.pone.0020400.

Jia, X. *et al.* (2019) 'High-density extracellular probes reveal dendritic backpropagation and facilitate neuron classification', *Journal of Neurophysiology*, 121(5), pp. 1831–1847. Available at: https://doi.org/10.1152/jn.00680.2018.

Lee, A.C.H., Yeung, L.-K. and Barense, M.D. (2012) 'The hippocampus and visual perception', *Frontiers in Human Neuroscience*, 6. Available at: https://doi.org/10.3389/fnhum.2012.00091.

Levy, D.R. *et al.* (2023) 'Mouse spontaneous behavior reflects individual variation rather than estrous state', *Current Biology*, 33(7), pp. 1358-1364.e4. Available at: https://doi.org/10.1016/j.cub.2023.02.035.

Lisman, J.E. and Jensen, O. (2013) 'The Theta-Gamma Neural Code', *Neuron*, 77(6), pp. 1002–1016. Available at: https://doi.org/10.1016/j.neuron.2013.03.007.

Lovick, T.A. and Zangrossi, H. (2021) 'Effect of Estrous Cycle on Behavior of Females in Rodent Tests of Anxiety', *Frontiers in Psychiatry*, 12, p. 711065. Available at: https://doi.org/10.3389/fpsyt.2021.711065.

Micevych, P.E. and Meisel, R.L. (2017) 'Integrating Neural Circuits Controlling Female Sexual Behavior', *Frontiers in Systems Neuroscience*, 11, p. 42. Available at: https://doi.org/10.3389/fnsys.2017.00042.

Pritschet, L. *et al.* (2020) 'Functional reorganization of brain networks across the human menstrual cycle', *NeuroImage*, 220, p. 117091. Available at: https://doi.org/10.1016/j.neuroimage.2020.117091.

Protopopescu, X. *et al.* (2008) 'Hippocampal structural changes across the menstrual cycle', *Hippocampus*, 18(10), pp. 985–988. Available at: https://doi.org/10.1002/hipo.20468.

Reddy, D.S. (2013) 'Neuroendocrine aspects of catamenial epilepsy', *Hormones and Behavior*, 63(2), pp. 254–266. Available at: https://doi.org/10.1016/j.yhbeh.2012.04.016.

Rizkjackson, A. *et al.* (2006) 'Effects of sex on object recognition and spatial navigation in humans', *Behavioural Brain Research*, 173(2), pp. 181–190. Available at: https://doi.org/10.1016/j.bbr.2006.06.029.

Rydström, K. (2020) 'Degendering Menstruation: Making Trans Menstruators Matter', in C. Bobel et al. (eds) *The Palgrave Handbook of Critical Menstruation Studies*. Singapore: Springer Singapore, pp. 945–959. Available at: https://doi.org/10.1007/978-981-15-0614-7_68.

Smarr, B., Rowland, N.E. and Zucker, I. (2019) 'Male and female mice show equal variability in food intake across 4-day spans that encompass estrous cycles', *PLOS ONE*. Edited by E.M. Mintz, 14(7), p. e0218935. Available at: https://doi.org/10.1371/journal.pone.0218935.

Wolcott, N.S. *et al.* (2022) 'Automated classification of estrous stage in rodents using deep learning', *Scientific Reports*, 12(1), p. 17685. Available at: https://doi.org/10.1038/s41598-022-22392-w.